mater.scichina.com link.springer.com

Published online 20 May 2022 | https://doi.org/10.1007/s40843-022-2037-4
Sci China Mater 2022, 65(8): 2217–2226

SPECIAL ISSUE: Flexible Intelligent Materials

Inkjet printing of 2D polyaniline for fabricating flexible and patterned electrochromic devices

Xiangyu Huang, Jie Chen, Hongjie Xie, Feixiang Zhao, Suna Fan* and Yaopeng Zhang*

ABSTRACT **Conjugated organic polymer (COP)-based electrochromic devices (ECDs) exhibit promising applications in digital and color displays. However, fabricating COP-based ECDs integrated with excellent electrochromic performance, customized patterns, and flexibility remains challenging. In this study, we report inkjet-printed, flexible, and patterned ECDs based on two-dimensional (2D) polyaniline (PANI) sheets, which are evenly dispersed in formic acid (FA) enabling high-precision, stable inkjet printing. The pristine lamellar structure of PANI sheets, which combine nanoscale thickness and an appropriate doping ratio, and the additive-free ink composition endow the printed PANI electrodes and ECDs with high performance. The fabricated PANI electrode exhibits a high optical contrast (76% at a wavelength of 750 nm), a good coloration efficiency (CE) of 259.1 $cm^2 C^{-1}$, and a short coloration/bleaching time (1.8/2.4 s), simultaneously integrated with pseudocapacitance and mechanical flexibility. Moreover, the 2D lamellar PANI ink developed in this study can be printed into various designed patterns, particularly for electrochemically controlled, addressable electrochromic displays. This work highlights 2D lamellar PANI as a promising electrochromic material for flexible and patterned ECDs.**

Keywords: inkjet printing, polyaniline, 2D sheets, electrochromic displays, flexible electronics

INTRODUCTION

Electrochromic material can change its optical properties as a result of electrochemical redox with ion insertion under an external potential, opening new possibilities for flexible displays [1,2], smart windows [3], and military camouflage [4]. Traditionally, electrochromic material is deposited on conductive substrates to fabricate electrochromic devices (ECDs) by magnetron sputtering [5], electrochemical deposition [1], spin-coating [6], and spray-coating [7]. These pioneering demonstrations cannot meet the requirements in flexible electrochromic electronics with an individual patterned design. Increasing research interest has been devoted to the printing technique, which can potentially reduce the overall process complexity and achieve high throughput without material waste [8,9]. As one of the printing techniques, inkjet printing offers a promising contactless deposition strategy to create digital and customized patterns on a myriad of substrates, including flexible thin films, which can meet the requirements in flexible electrochromic electronics with individual patterned design [10–14].

Inkjet-printed (IJP) patterns require a stable jetting of single droplets without nozzle clogging issues. Thus, the inkjet printing ink should have excellent electrochromic performance, an appropriately sized dispersed phase, and suitable viscosity and surface tension [15,16]. Among various electrochromic materials, conjugated organic polymers (COPs), exemplified by polyaniline (PANI) and polythiophene derivatives, have attracted significant attention in ECDs due to their diverse colors, simple processing, low manufacturing costs, and intrinsic flexibility compared with their inorganic counterparts [17,18]. In general, bulk COPs are dissolved in polar solvents after synthesis to optimize the fluid properties of the ink for printing [19–21]. For instance, polyindenofluoren-8-tryarylamine (PIF8-TAA) was dissolved in 3-chlorotoluene, with tetralin as an additive, for inkjet printing. However, the optical contrast of the printable ECDs was only 24%, which is much lower than that of the devices fabricated by conventional deposition approaches [19]. In another study, PANI had to be dissolved in dimethyl sulfoxide (DMSO) with the addition of a dopant and ultrasonicated for 1 h to obtain a stable ink [20]. These processes destroyed the condensed COP structure and morphology, influencing ion diffusion in the COPs and, thus, the electrochromic performance of the ECDs [17]. On the other hand, to suppress the coffee-ring effect, inkjet printing inks are usually mixed with surfactants or polymer stabilizers (e.g., ethylene glycol [22] or Triton X-100 [23]) and/or added with secondary solvents [24]. These methods result in residual additives in the printed ECDs, which need to be removed by high-temperature annealing [25]. This process may deteriorate most flexible substrates, making it unsuitable for inks containing COP components. Hence, developing high-quality inkjet printing inks without additives is vital.

To overcome these limitations, constructing low-dimension COPs (e.g., zero-dimensional (0D) nanoparticles [26–28] and 1D nanotubes [29]) helps create inks with stable dispersity and reliable optoelectronic performance for direct inkjet printing. In these cases, electron transfer between adjacent 0D or 1D structures was hindered by the limited contact area [30], and these structures might be unsuitable for flexible devices because 0D or 1D COPs are easy to break under the bending state [31]. In this

State Key Laboratory for Modification of Chemical Fibers and Polymer Materials, College of Materials Science and Engineering, Donghua University, Shanghai 201620, China
* Corresponding authors (emails: fsn@dhu.edu.cn (Fan S); zyp@dhu.edu.cn (Zhang Y))

study, we propose that 2D lamellar COPs are promising for high-performance and flexible IJP ECDs because of the much larger contact area between adjacent 2D nanosheets and the retardation for mechanical deformation. In addition, compared with the bulk forms, 2D lamellar COPs provide an increased specific surface ratio; thus, interface areas with the electrolyte are larger, leading to faster ion diffusion [32]. However, as strategies for bottom-up synthesizing 2D COPs are sophisticated [33–35], they have not been developed for high-quality inks and reliable inkjet printing in optoelectronic applications and ECDs.

Herein, we successfully fabricated 2D lamellar PANI-based ink without any additives and then IJP electrochromic patterns with high printing efficiency and uniformity. Moreover, the intrinsic lamellar structure of PANI could be preserved after exfoliation and stored in our ink formulation. The printed patterns exhibited good electrochromic performance, with a high optical contrast of 76% at a wavelength of 750 nm, a rapid coloration/bleaching speed (1.8/2.4 s), and a high coloration efficiency (CE) of 259.1 $cm^2\ C^{-1}$. We further demonstrated a flexible ECD with a customized pattern and a seven-segment display with independent pixels, which could potentially be integrated with flexible substrates for next-generation ECDs and future displays with low-power consumption.

EXPERIMENTAL SECTION

Materials

Aniline (J&K, 99+%) was distilled before use. *p*-Toluenesulfonic acid (pTSA, Sigma-Aldrich), ethanol (Sigma-Aldrich), isopropanol (IPA, Sigma-Aldrich), DMSO (Sigma-Aldrich), formic acid (FA, Sinopharm Chemical Reagent Shanghai Co., Ltd.), $LiClO_4$ (Aladdin), propylene carbonate (PC, Sinopharm Chemical Reagent Shanghai Co., Ltd.), and poly(methylmethacrylate) (PMMA, Aladdin) were used without further purification. All the chemicals were of analytical reagent grade or higher. Indium tin oxide (ITO)/glass and ITO/polyethylene terephthalate (PET, 6 Ω sq^{-1}, South China Science and Technology Co., Ltd.) were sequentially cleaned by acetone, ethanol, and deionized water. The PET film was cut into pieces and cleaned with ethanol and deionized water before use. The silver paste used for the screen-printed conductive lines was purchased from Shenzhen D-MAX Technology Co., Ltd. (Shenzhen, China).

Fabrication of 2D lamellar PANI ink

The PANI film was synthesized *via* a modified method [32]. Briefly, a homemade three-electrode electrochemical cell was used to deposit the PANI film doped with pTSA on an ITO glass under potentiostatic conditions. ITO, a platinum plate, and a saturated calomel electrode (SCE) were used as the working electrode, counter electrode, and reference electrode, respectively. The electrolyte was a 0.5 mol L^{-1} pTSA solution containing 0.1 mol L^{-1} aniline, and the applied potential for PANI polymerization was 0.75 V *versus* the SCE. After polymerization, the pTSA-PANI film was released from the ITO glass into ethanol, and then washed twice with ethanol and deionized water. Finally, the pTSA-PANI powders were dried at room temperature until a constant weight was achieved. To formulate PANI inks, the pTSA-PANI powders were redispersed into FA, followed by ultrasonication, and then the supernatant was collected for use in the inkjet printing process. The final concentration of PANI was approximately 5.5 mg mL^{-1}.

Inkjet printing process

Before printing, the PANI ink was loaded onto the inkjet printing system (JETLAB 4, Microfab, USA). Printing was achieved through piezoelectric nozzles with a diameter of 80 μm at a 250 Hz vibrational frequency. The three-axis movement and the values of the printing parameters were computer-controlled, and the dimension of the ink drops was controlled based on a direct drop observation, which was performed by a horizontal camera. At a sinusoidal pulse with a peak voltage of 45–50 V and a period of 38–42 μs, ink drops with a diameter of 40–60 μm were obtained. Consequently, the script used for printing was set to obtain a drop spacing of 50 μm to achieve complete coverage of the substrate. The substrate holder was heated to 35°C to accelerate solvent evaporation. Samples were printed onto bare PET films for the resistance and thickness characterization and onto ITO/PET for electrochemical and electrochromic characterizations, respectively. These samples were printed into rectangular patterns (10 mm × 5 mm) with different layers and dried in air. Alternatively, the samples with a larger printed size of rectangular patterns (20 mm × 10 mm) were assembled into flexible ECDs.

Assembly of flexible PANI ECDs and a seven-segment display device

After inkjet printing PANI patterns onto ITO/PET, the gel electrolyte was cast on the PANI patterns, and another ITO/PET was coated on the gel electrolyte layer. The polymer gel electrolyte contained 1 mol L^{-1} $LiClO_4$/PC solution and 10 wt% PMMA (relative to the $LiClO_4$/PC solution). Here 200-μm-thick tapes were used as the spaces to control the thickness of the electrolytes. For the assembly of a seven-segment display, the silver paste was screen-printed on the bare PET films, and then dried at 80°C in an oven for 30 min. Subsequently, the designed patterns of PANI were printed onto the silver lines. Finally, the seven-segment electrochromic displays were formed by the same assembly process used to obtain flexible ECDs.

Structural characterization

X-ray reflectivity (XRR) patterns were measured using an X-ray diffractometer (D2 Phaser, Bruker). The morphologies of the lamellar PANI film and printed PANI patterns were studied using field emission-scanning electron microscopy (SEM) (SU8000, Hitachi) and atomic force microscopy (AFM) (Shimadzu SPM-9700HT). The morphology and structure of 2D PANI in ink were characterized concurrently by transmission electron microscopy (TEM) and selected area electron diffraction (SAED) using a JEOL JEM-2100 electron microscope operated at 200 kV. A drop of PANI ink was diluted in ethanol and then transferred to lacey-carbon-coated grids and freshly cleaved mica, respectively, for TEM and AFM characterizations. Fourier transform infrared (FTIR) spectra were recorded by a Nicolet 6700 Fourier transform spectrometer. X-ray photoelectron spectroscopy (XPS) (Axis Supra, Shimadzu) was conducted to characterize the chemical composition and doping level of the samples. The thickness of the printed PANI patterns was measured *via* a profilometer (Tencor PLA 10).

Ink property measurement of the PANI ink

The density of the PANI ink was calculated by the weighing method. The surface tension and wettability of the PANI ink were evaluated using a contact angle goniometer (CA, OCA40

Micro, Dataphysics Ltd., Germany). The viscosity was measured by an RS150 rheometer (Thermo Haake, Germany) at 25°C. The physical stability of 2D PANI in an FA suspension was analyzed by a multi-sample stability analyzer (Turbiscan TOWER, Formulaction Co., L'Union, France) at 25°C for 15 days. The sample in a special cuvette holder was scanned from the bottom to the top of the suspension by a pulsed near-infrared light source (λ = 880 nm). During this process, the transmission detector (at 180°) received the transmitted light through the sample, while the backscattering detector (at 45°) detected the scattered light from the sample. The transmission and backscattering data were collected at position change intervals of 40 μm. Dynamic light scattering measurements were performed with a particle size analyzer (Litesizer 500, Anton Parr). Samples were tested in quartz cuvettes with a 10-mm path length and were equilibrated to 25°C for 60 s before the measurement.

Electrochemical and electrochromic measurements

A Keithley 236 sourcemeter was used to test the sheet resistance of the printed PANI using the four-point probe method. Electrochemical measurements were carried out using an electrochemical workstation (PGSTAT204, Metrohm Autolab) in 1 mol L^{-1} $LiClO_4$/PC electrolyte in a three-electrode electrochemical cell with the IJP PANI film as the working electrode, a platinum plate as the counter electrode, and an SCE as the reference electrode. Electrochemical impedance spectroscopy (EIS) was conducted with a 1-mV perturbation amplitude from 0.5 to 10^5 Hz. The PANI film transmittance spectra were collected using an ultraviolet-visible-near-infrared (UV-vis-NIR) spectrophotometer (UV3600, Shimadzu) at room temperature while applying potentials *via* the Autolab electrochemical workstation. All film spectra were baseline subtracted using the spectrum of the bare electrode, and the spectra of ECDs were collected relative to air. A homemade mechanical device was used to achieve the bending/unbending cycles of the flexible ECDs, and the curvature radius was set as 4 cm.

RESULTS AND DISCUSSION

Preparation of 2D lamellar PANI inks without additives

Highly oriented lamellar PANI, as the core functional component in the PANI ink, was obtained through electrochemical polymerization (Fig. 1a), in which pTSA served as a dopant and interacted with the PANI molecular chains to guarantee the lamellar structure of PANI film [30,32]. The obtained pTSA-PANI is composed of ordered layers stacked parallel to the surface of the substrate, as clearly demonstrated by the sharp Bragg peaks of the XRR patterns in the [001] direction (Fig. S1) and the SEM and AFM images (Fig. 1b, c and Fig. S2). In addition, the thickness of these stacked lamellar sheets was at least 1.14–1.24 nm (Fig. 1d), which is consistent with the interlayer distance spacing of PANI film (1.27 nm) calculated by XRR (Fig. S1). This hierarchical structure facilitates ion diffusion, thus improving the electrochromic properties of ECDs [32]. Subsequently, we used a liquid-phase exfoliation method to break down the lamellar PANI film into 2D PANI sheets, which were composed of lamellar PANI with single-molecule thickness [32]. According to the Hansen solubility parameter theory [36–38], a few solvents, including IPA, DMSO, and FA, were selected to exfoliate and disperse the 2D lamellar PANI. However, PANI tended to agglomerate and sediment in IPA (Fig. S3a) because of its lowest polar Hansen parameters among the solvents (Table S1). In addition, although PANI can be dispersed in DMSO, whose polarity is stronger than that of IPA, the obtained dispersion was black (inset of Fig. 1e and Fig. S3b), which is a characteristic of the de-doped PANI in the emeraldine base (EB) form and not suitable for printing ECDs without any other process [39]. Therefore, polar protic solvents, with a Hansen solubility parameter similar to that of the emeraldine salt, are the best choice to disperse lamellar PANI and keep PANI in a doped state [40]. Successfully, the 2D lamellar PANI was well-dispersed in FA and appeared to be stable for at least half a month, and it was characterized *via* continuous backscattering curves (Fig. S4). In particular, the ink of PANI in FA shows an intense green (inset of Fig. S3c), suggesting the doping state of PANI in dispersion. This result was additionally confirmed by the UV-vis spectra, in which bands at 420–436 and 745–765 nm were ascribed to the polaron and bipolaron transitions, respectively (Fig. S3c) [41].

To study the molecular configuration of PANI, as well as the dispersion mechanism, the FTIR spectra were applied to characterize the as-prepared pTSA-PANI film and PANI sheets dried from the FA ink (Fig. 1f). The FTIR spectra of these samples were found to display the characteristic peaks of PANI. The broad band centered at 3400 cm^{-1} and the peaks located at 1300 and 1245 cm^{-1} are attributed to the N–H stretching vibration of an aromatic amine, the C–N stretching vibration with an aromatic conjugation, and the C=N stretching vibration, respectively [42]. The peaks located at 1475, 1130, and 816 cm^{-1} correspond to the C=C stretching vibration of the benzenoid ring and in-plane and out-of-plane bending of the C–H group, respectively [42]. In addition, the peaks centered at 2958, 2924, and 2854 cm^{-1} originate from the hydrogen bonds formed between the counter-anion and –NH groups or neighboring chains [43,44]. These hydrogen bonds help to maintain the lamellar PANI structure after dispersion in FA ink. In the "fingerprint" area of the FTIR spectra (Fig. S5), the characteristic peaks of the S=O stretching vibration of the $-SO_3H$ groups, located at 1378 and 1037 cm^{-1}, are present in the as-prepared pTSA-PANI film and PANI sheets from the FA ink [45]. This result reconfirms that pTSA-PANI maintains its doped state even after liquid-phase exfoliation. Additionally, two new peaks located at 1639 and 1409 cm^{-1}, which are attributed to the C=O stretching vibration and –OH bending of carboxylic acid, respectively, can be observed in the dispersed PANI sheets (Fig. S5) [46]. This result indicates that FA is inserted into the lamellar PANI and may act as a dopant in the PANI molecule. To confirm this hypothesis, XPS measurements were conducted to determine the oxidation state of PANI (Fig. 1g). The characteristic peaks located at 401.5 and 402.4 eV are attributed to $-NH_2^+-$ and $-NH^+=$, verifying the doping state of PANI [47]. Furthermore, the doping ratio of PANI sheets from ink, 66.4%, is higher than that of the pTSA-PANI film (44.9%) (Table S2). This result verified that the doping level of PANI was improved after being dispersed by FA, which is consistent with the FTIR spectra (Fig. 1f).

More importantly, the original lamellar structure of PANI was retained in the FA dispersion, as observed in the TEM (Fig. 1h and Fig. S6) and AFM images (Fig. 1i and Fig. S7). This result might be due to the in-plane interchain interactions and hydrogen bonds between counter-anions and PANI molecular chains [30], as confirmed by the FTIR spectra (Fig. 1f). In

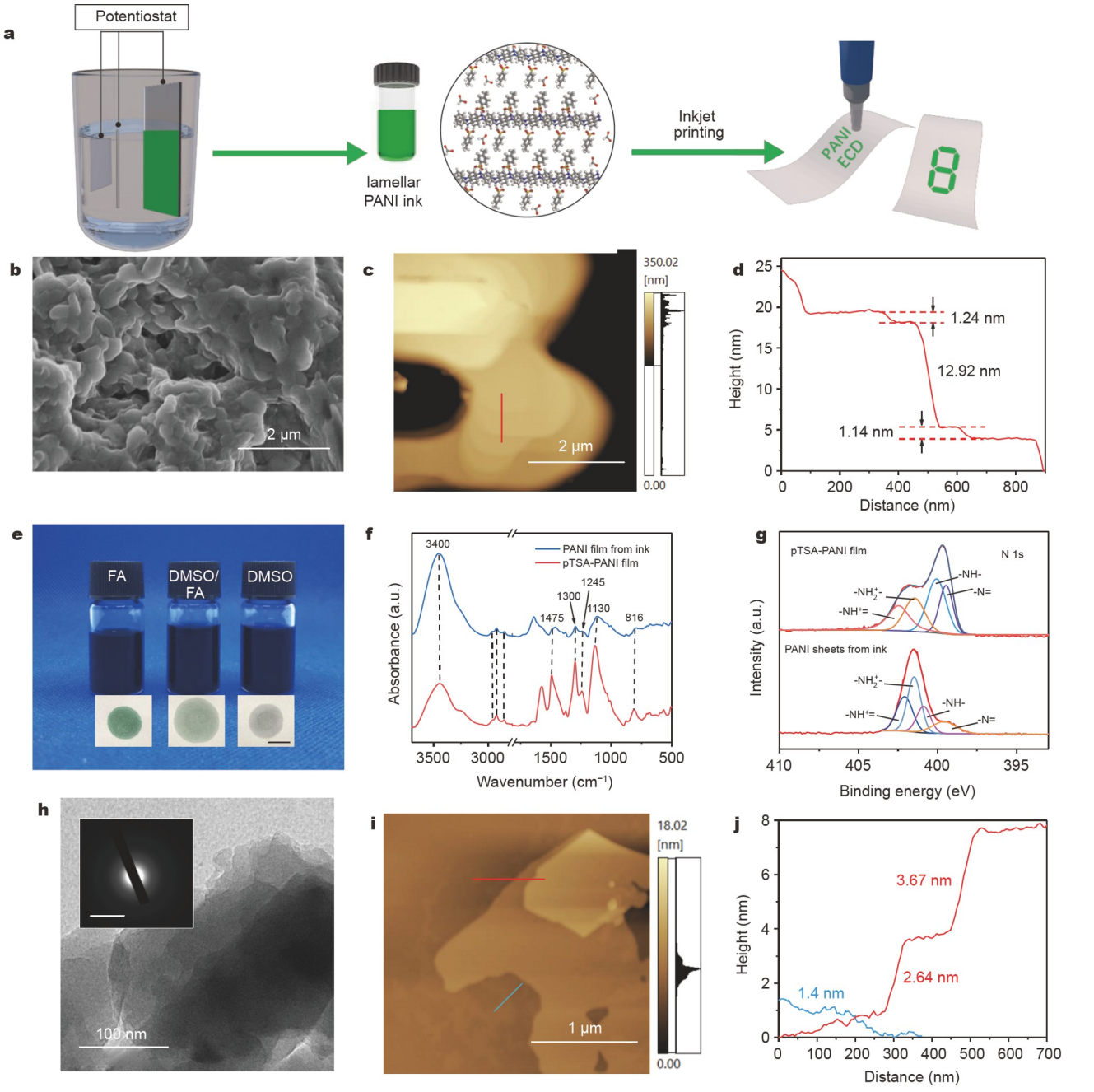

Figure 1 Fabrication of the 2D lamellar PANI ink. (a) Schematic illustration of the preparation of flexible and patterned electrochromic electrodes. SEM (b) and AFM (c) images of the as-prepared pTSA-PANI film through electrochemical polymerization. (d) Height profile along the red line indicated in (c). (e) Photos of various PANI inks dispersed in different solvents. Inset: photos of filter papers wetted by one drop of different PANI dispersions. Scale bar: 1 cm. FTIR spectra (f) and XPS spectra of the N 1s peaks (g) of pTSA-PANI film and PANI sheets from FA ink. TEM (h) and AFM (i) images of lamellar PANI sheets dispersed in FA. Inset of (h): SAED pattern. Scale bar: 5 nm^{-1}. (j) Height profiles along the red and blue lines indicated in (i).

addition, no obvious diffraction rings are observed in the SAED pattern of PANI (inset of Fig. 1h), confirming the amorphous nature of PANI. This attribute benefits ionic penetration and transportation, facilitating the electrochromic response [32]. The thickness and lateral size of the lamellar PANI were 1–3 nm and 1.36 μm, respectively, indicating that a single layer or a few layers of PANI sheets were fabricated (Fig. 1i, j and Figs S7 and S8), based on the interlayer spacing (12.7 Å). Therefore, we believe that PANI ink without additives, which maintained its original 2D lamellar structure and doped state, was successfully prepared through simple liquid-phase exfoliation for the first time.

Inkjet printing of PANI inks

Contact angle tests were performed to evaluate the wetting ability of the FA-formulated PANI ink on different substrates. The ink displayed excellent wetting characteristics on various substrates, including Si wafers, PET film, glass slides, and ITO/PET, as is evident by the contact angles of approximately 20° and especially 12.6° on ITO/PET (Fig. 2a and Fig. S9), which is

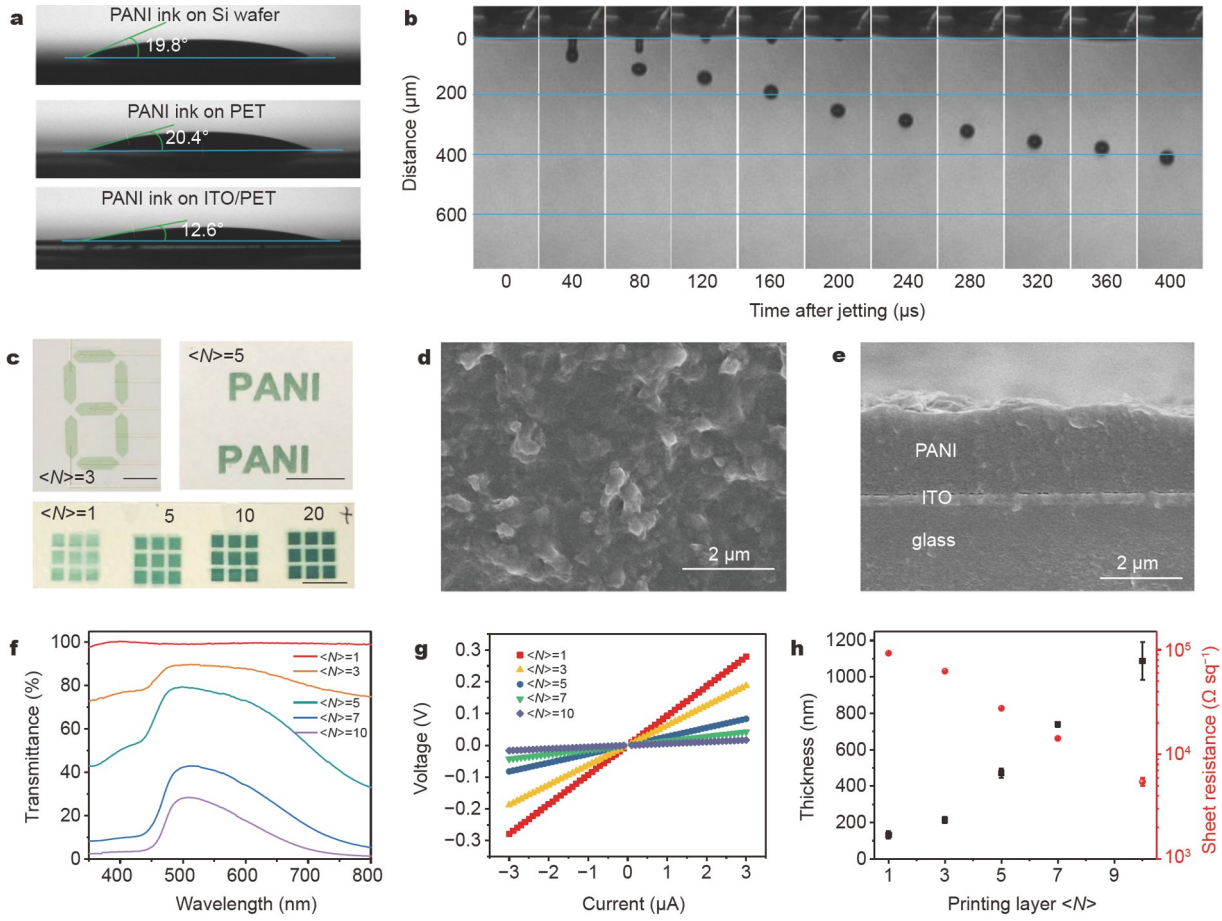

Figure 2 Inkjet printing of 2D PANI ink. (a) Contact angles of the lamellar PANI ink spread on different substrates. (b) Stroboscopic images of inkjet droplets demonstrating the stable ink jetting performance. (c) Photographs of various IJP PANI patterns. Scale bars: 1 cm. Surface (d) and cross-sectional (e) SEM images of IJP PANI film on ITO glass with printing layers of <*N*> = 20. (f) Optical transmittance spectra of PANI film with different printing layers. (g) Current-voltage (*I*-*V*) curves of the films printed on a bare PET substrate. (h) Film thickness and sheet resistance of the films printed on a bare PET substrate.

crucial for printing a functional pattern on the flexible transparent electrode. This behavior is due to the lower surface tension of the PANI ink (35.5 mN m^{-1}) (Fig. S10a and Table S3) compared with that of a Si wafer or glass (~36 mN m^{-1}), PET (~48 mN m^{-1}) [48], and ITO/PET (~68.2 mN m^{-1}) [49]. To demonstrate the utility of PANI ink in inkjet printing, ink formulation was performed using the inverse Ohnesorge number, *Z* [15]:

$$Z = \frac{\sqrt{\rho\gamma d}}{\eta}, \quad (1)$$

where ρ, γ, d, and η represent the ink density, surface tension, nozzle diameter, and viscosity, respectively. The lamellar PANI in FA ink showed a viscosity of 50.4 mPa s, and the *Z* value was evaluated to be 1.2 (Fig. S10b, Table S3), which fell in the range between 1 to 10 required to form stable and separated droplets [15]. As expected, stable jetted droplets are formed, well-directed, and constantly jetted from the nozzle without satellite droplets (Fig. 2b and Fig. S11), which is the foundation for uniform printing. Then, various customized patterns with different inkjet printing layers <*N*> were printed on ITO/PET, including a seven-segment display, letters, and arrays (Fig. 2c). Notably, no obvious coffee-ring effect is apparent in the printed patterns in this work. This result can be attributed to the following factors: the Marangoni flow caused by the FA solvent with high boiling point and lower surface tension [16,50]; the heating of the substrate holder during the printing process to accelerate solvent evaporation and avoid an inhomogeneous deposition. As a result, the printed PANI formed stacked lamellae and exhibited continuous coverage over the substrate (Fig. 2d, e and Figs S11–S13), which benefits ionic transport and charge transfer.

The optical and electronic properties of the PANI film were evaluated by UV-vis spectra and a four-point probe resistance measurement technique. The optical transmission of PANI with <*N*> = 1 relative to the bare substrate is approximately 100% and highly transparent (Fig. 2f). For a printing layer of <*N*> = 5, the transmittance of the film at 550 nm is 77% and appears green (Fig. 2c, f). Then, as expected, the optical transmission of PANI decreased sharply to less than 40% with printing layers of <*N*> = 7 and 10. In addition, the linear current-voltage relationship (Fig. 2g) of the various films demonstrated the Ohmic behavior of IJP PANI, and the sheet resistance values spanned from 10^4 to 10^3 Ω sq^{-1} with increasing printing layers (Fig. 2h). This result is due to the decreased defect in conductive pathways within printed films with increasing printing layers. Hence, optoelectronic thin films with various optical transmissions and resistance values can be easily fabricated by adjusting the printing

layer. Furthermore, the inkjet printing technique based on our PANI ink offers a simple route to printing electrochromic films on flexible substrates, which are essential components of flexible patterned ECDs.

Electrochemical and electrochromic performance of printable PANI sheet patterns

The electrochromic performance of the IJP PANI film with different values of <*N*> was measured in 1 mol L^{-1} $LiClO_4$/PC electrolyte through spectra-electrochemistry. Derived from cyclic voltammetry (CV) curves, at a scan rate of 30 mV s^{-1} (Fig. 3a), the anodic and cathodic peak currents of the PANI film increased with the number of printed layers, indicating that the capacity increases in proportion to this number. Transmittance plots measured at different potentials show an electrically induced modulation of optical density in a wide range, from 400 to 800 nm (Fig. 3b and Fig. S14, Table S4), associated with the visible color change (Fig. S15). The maximum transmittance modulation, ΔT (defined as the optical contrast), of the PANI film, with <*N*> = 3, 5, and 7, was 66%, 76%, and 74%, respectively, at 750 nm. These high optical contrasts are due to the sufficient contact between the PANI film and electrolyte, which results from the stacked lamellae on the surface of the printed PANI film (Fig. 2d and Fig. S13). For printing PANI film with <*N*> = 10, ΔT then decreased to 55% because of the low transmittance (Fig. 2f). The switching time is another important factor for electrochromic material, and the response of the transmittance at 750 nm was measured from −0.4 and 0.6 V (Fig. 3c). The coloration/bleaching time (t_c/t_b), defined as the time to reach 90% of the optical contrast [17], was extracted to be 2.2/4.0, 1.8/2.4, and 1.8/6.2 s for the PANI film with <*N*> = 3, 5, and 7, respectively (Fig. S16, Table S4), which are faster than previously reported values for PANI electrochromic material and WO_3 material [22]. Note that the discontinuity of the conductive pathway within the printed films with <*N*> = 3 may lead to a longer coloration/bleaching time (Fig. S12b).

As an effective criterion for evaluating the electrochromism coloration efficiency (CE), η is defined as the change in the

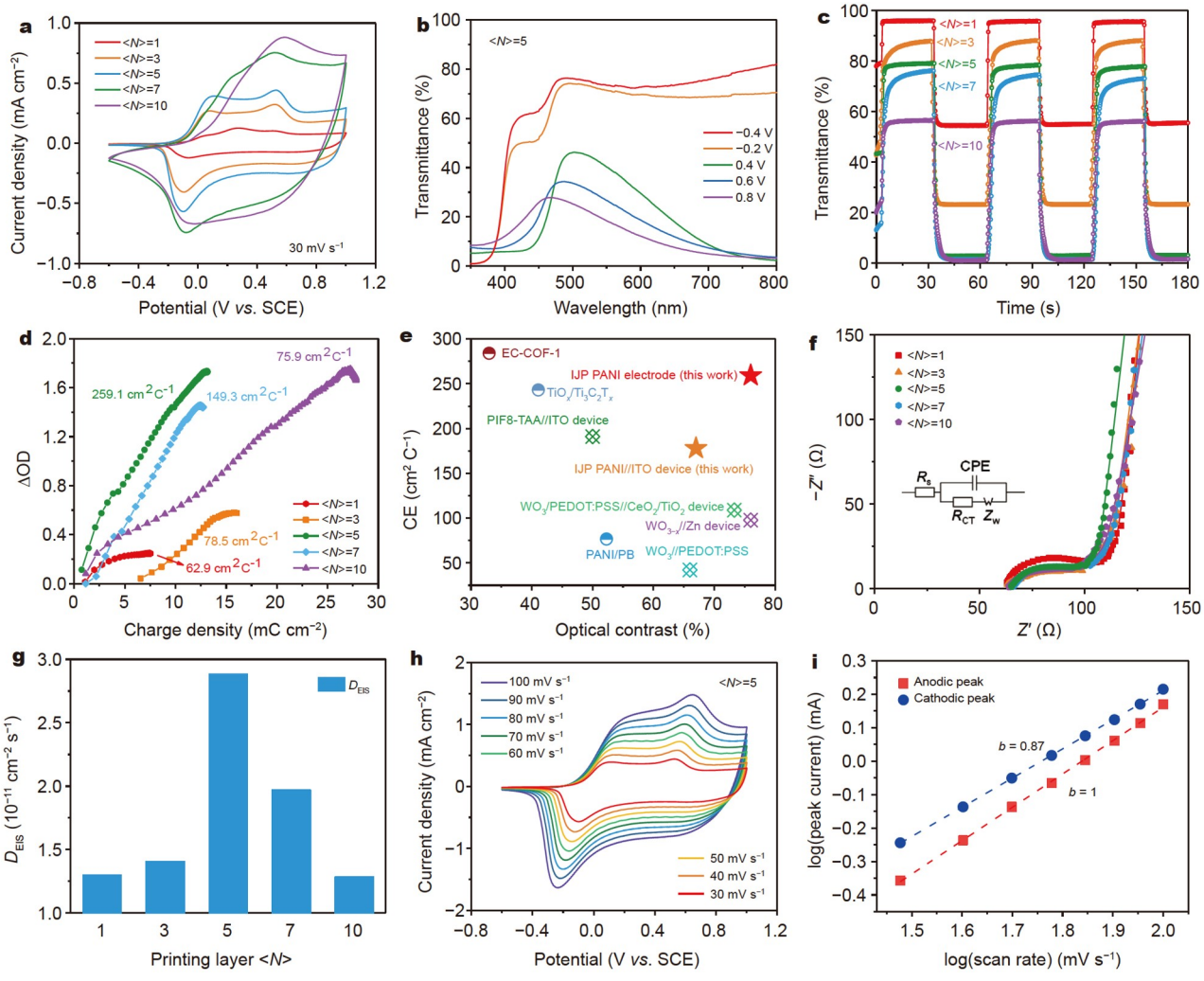

Figure 3 Electrochemical and electrochromic properties of the IJP PANI film. (a) CV curves measured in 1 mol L^{-1} $LiClO_4$/PC electrolyte. (b) Optical transmittance spectra of the PANI film printed with <*N*> = 5 under different potentials. (c) Coloration/bleaching switching behavior of the IJP PANI film with different printing layers. (d) Optical density change (ΔOD) as a function of the injected charge density. (e) Comparison of the CE value and optical contrast of the IJP PANI film, device, and other electrochromic materials previously reported [19,22,31,51–54]. Nyquist plots (f) and diffusion coefficients (D_{EIS}) (g) of the IJP PANI films. (h) CV curves of the PANI film printed with <*N*> = 5 at different scan rates. (i) Log(*i*)-log(*v*) plot of the anodic and cathodic current responses.

optical density of IJP PANI film in the colored and bleached states (transmittance T_c, T_b, respectively) induced by the charge density (Q, charge intercalated into PANI anode material per unit area) [17]:

$$\Delta OD = \log\left(\frac{T_b}{T_c}\right), \quad (2)$$

$$\eta = \frac{\Delta OD}{Q}. \quad (3)$$

When the printed layers are less than 5, the PANI film displays a lower CE value because the conductive pathway within the films is discontinuous and incomplete (Fig. S12a, b), leading to an incomplete interaction between the lamellar PANI. This result was reflected by the higher sheet resistance of the samples with fewer printing layers (Fig. 2h). However, increasing the number of printing layers can significantly improve this condition. For example, the IJP PANI film with <N> = 5 and 7 had high CE values of 259.1 and 149.3 cm^2 C^{-1}, respectively, at a wavelength of 750 nm (Fig. 3d, Table S4). This result indicates that small amounts of charge insertion/extraction can result in large optical modulation. This result also guarantees the long-term electrochemical stability of the IJP PANI film, which maintained 80% optical contrast after 1000 electrochromic cycles (Fig. S17a). Further increasing the number of printing layers, the CE value tends to decrease with decreasing optical contrast (Table S4).

To compare the present work with the literature (Fig. 3e, Table S5), we found that our printable 2D PANI sheets showed better electrochromic performance than other COPs, including the polystyrene sulfonate (PSS)-doped PANI/Prussian blue composite [51], PIF8-TAA [19], and PSS-doped poly(3,4-ethylenedioxythiophene) (PEDOT:PSS) [22]. Moreover, printable 2D PANI sheets have advantages in the CE value and optical contrast compared with WO_3 material [22,52,53], which is well-explored as one of the representative electrochromic materials. Additionally, our 2D PANI sheets display similar CE values and higher optical contrast than several pioneer electrochromic materials, such as conjugated organic framework material [54] and MXene-based material [31]. This comparison indicates that the lamellar PANI ink and its printed electrode reported in this study have excellent electrochromic performance, and this technique endows PANI film with customization and patterning, which exhibits advantages for next-generation ECDs.

Electrochemical mechanism in printable PANI sheet patterns

To further explore the ion diffusion behavior of the printable PANI sheets, EIS was measured and analyzed (Fig. 3f). The ion diffusion coefficient, D, which represents the kinetics of ion insertion/extraction in the electrochromic film, can be extracted from the Warburg region of EIS measurements (D_{EIS}) [31]:

$$D_{EIS} = \frac{R^2T^2}{2A^2n^4F^4C_0^2\sigma^2}, \quad (4)$$

where R is the gas constant, T is the absolute temperature, A is the surface area of the electrode, n is the number of electrons transferred per unit reaction, F is the Faraday constant, C_0 is the concentration of the counterion, and σ is the slope of Z' (real axis of impedance) against $\omega^{-1/2}$ (angle frequency). As shown in Fig. 3g and Table S6, the D_{EIS} values of the PANI film with different layers (<N> = 1, 3, 5, 7, and 10) were 1.30×10^{-11}, 1.40×10^{-11}, 2.88×10^{-11}, 1.97×10^{-11}, and 1.28×10^{-11} cm^2 s^{-1}, respectively. The ion diffusion coefficient, D_{EIS}, was within the same order of magnitude for all PANI films, which shows the stable electrochemical performance of the printable PANI sheets. Thus, the switching time is within the same range for all the samples, i.e., of a few seconds. The <N> = 5 sample shows the highest D_{EIS} value, indicating a faster ion insertion/extraction, which is consistent with the shorter coloration/bleaching time (1.8/2.4 s). The Nyquist plots from EIS do not change considerably as the PANI thickness increases from <N> = 1 to 10 (Fig. 3f), and the charge-transfer resistance (R_{CT}) ranges from 19.8 to 36.0 Ω (Table S6). These results indicate that the multilayer stacking does not significantly decrease the charge-transfer rate at the interface of the PANI film and electrolyte [31].

Furthermore, sweep voltammetry measurements at scan rates from 30 to 100 mV s^{-1} were used to provide deeper insight into the electrochemical kinetics (Fig. 3h and Fig. S18). All PANI films display anodic and cathodic peaks that are consistent with the reported leucoemeraldine base (LB)/emeraldine salt and EB/pernigraniline salt (PS) transitions [55]. The CV curves of the PANI film with different printing layers maintained a similar shape with a shift in the anodic and cathodic peaks with increasing scan rate (Fig. 3h), illustrating a stable electrochemical performance. The currents of the anodic and cathodic peaks (i) depend on the sweep rate (v) and follow Equation (5) [56]:

$$i = av^b. \quad (5)$$

In the plot of the linear log(i) *versus* log(v), the kinetics shows a surface-controlled capacitor-like behavior for the slope of b = 1, and a diffusion-controlled process is observed for b = 0.5 [56]. The b value for the anodic and cathodic peaks is 1 and 0.87 (Fig. 3i), respectively, indicating that the redox processes of the PANI film with <N> = 5 are dominated by pseudocapacitive kinetics. The pseudocapacitance behavior of the redox reaction endows the PANI film with a fast coloration/bleaching process (1.8/2.4 s, <N> = 5) (Fig. 3i and Fig. S18). Moreover, the specific capacitances of the PANI film with <N> = 5, calculated from the charge-discharge curves (Fig. S19), were approximately 748, 696, 609, and 463 F g^{-1} at current densities of 1, 2, 4, and 8 A g^{-1}, respectively. These results demonstrate the potential application of the printed PANI film in the field of multifunctional electrochromic energy devices.

IJP PANI ECDs for flexible electronics and display

We assembled printable PANI sheets into ECDs to test the performance of the overall device in practical applications. Under potentials of 1.5 and −1.5 V, the optical contrast of the PANI ECDs with <N> = 5 at 750 nm was 67% relative to air (Fig. 4a), which is smaller than that from three-electrode tests (Fig. 3b). The lower optical contrast resulted from assembling the ECDs in a sandwich structure, in which the IJP PANI, gel electrolyte, and bare ITO/PET act as the electrochromic layer, ion transport layer, and counter-electrode layer, respectively. These additional components in ECDs increased the intensity of light scattering [57], resulting in lower optical contrast. Simultaneously, the ECD needs a larger potential window to drive ion transport in the gel electrolyte and PANI film; hence, the decrease in the CE value of the ECDs is associated with a longer coloration/bleaching time. For example, the coloration/bleaching time and CE value of ECDs with <N> = 5 were 1.2/3.8 s and

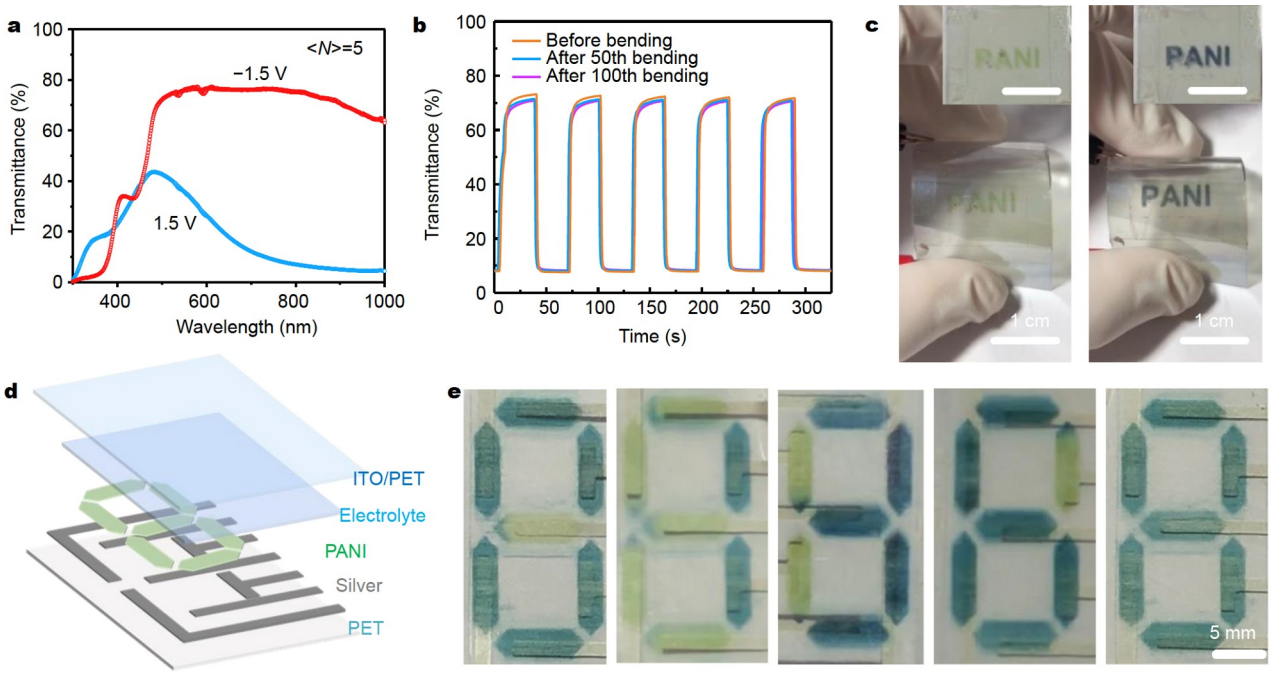

Figure 4 Demonstration of various PANI ECDs. (a) Optical transmittance spectra (relative to air) of the PANI ECDs with <*N*> = 5 under different potentials. (b) Electrochromic switching behaviors of the PANI ECD with <*N*> = 5 after 100 bending cycles. The bending curvature is 4 cm. (c) Electrochromic switching of the patterned ECDs in the bending and unbending states (inset) from the bleached state (−1.5 V) to the colored state (1.5 V) (from left to right). Schematic illustration (d) and digital photos of a seven-segment display (e), in which seven silver conductive lines screen-printed on the bare PET were set to control the individual IJP PANI segment.

177.9 $cm^2\ C^{-1}$, respectively (Fig. 4b and Fig. S20). However, the IJP ECDs based on our 2D lamellar PANI ink still showed the advantages of a higher CE value and optical contrast compared with other reported IJP ECDs (Fig. 3e). Moreover, the optical contrast of the printed ECDs remained at 96% after 100 bending cycles with a curvature radius of 4 cm (Fig. 4b and Fig. S21a, b). Additionally, the IJP ECDs showed electrochemical stability after either tensile testing of 40 N for 15 min or manual torsion for 50 iterations (Fig. S21c–f). Another important advantage of inkjet printing is to realize the rapid customization of various patterns. As shown in Fig. 4c, a printed ECD with a "PANI" letter pattern was fabricated and displayed excellent electrochromic performance even in the high bending state, under potentials of 1.5 and −1.5 V. This result further demonstrates the good stability and mechanical flexibility of the printable PANI sheets and their ECDs.

The versatile and generalized strategy introduced in this study allows the printable 2D lamellar PANI ink to be used for electrochemically controlled, addressable electrochromic displays. Seven individual PANI pixels were inkjet printed sequentially to construct a seven-segment display and were addressed by a screen-printed silver circuit (Fig. 4d). This ECD displayed different patterns to represent numbers, such as "0", "1", and "3", by independently controlling the color of the PANI pixels (Fig. 4e). This capability provides a new concept for flexible and customized electrochromic displays and opens the possibility of using COPs in the fields of flexible displays, smart windows, and next-generation electronics.

CONCLUSIONS

In summary, we demonstrated a printable 2D lamellar PANI ink without additives, which can be stored stably for at least half a month, for inkjet printing of high-performance ECDs. These ultra-thin PANI sheets of approximately 1–3 nm thickness, with a pristine lamellar structure and lateral size of 1.36 μm, are stably dispersed in an FA solvent, which also acts as a dopant of PANI molecules. The printed PANI electrodes integrate excellent electrochromic performance, such as an optical contrast of 76% at 750 nm, a short coloration/bleaching time of 1.8/2.4 s, and a good CE of 259.1 $cm^2\ C^{-1}$, with pseudocapacitive behavior and mechanical flexibility. Furthermore, an electrochemically controlled, addressable electrochromic display was demonstrated by combining the 2D PANI ink with a screen-printed silver circuit, providing new possibilities for ECDs for next-generation flexible and patterned electronics.

Received 6 January 2022; accepted 16 March 2022; published online 20 May 2022

1 Kaissner R, Li J, Lu W, *et al.* Electrochemically controlled metasurfaces with high-contrast switching at visible frequencies. Sci Adv, 2021, 7: eabd9450
2 Wang Y, Wang S, Wang X, *et al.* A multicolour bistable electronic shelf label based on intramolecular proton-coupled electron transfer. Nat Mater, 2019, 18: 1335–1342
3 Strand MT, Hernandez TS, Danner MG, *et al.* Polymer inhibitors enable >900 cm^2 dynamic windows based on reversible metal electrodeposition with high solar modulation. Nat Energy, 2021, 6: 546–554
4 Ergoktas MS, Bakan G, Kovalska E, *et al.* Multispectral graphene-based electro-optical surfaces with reversible tunability from visible to microwave wavelengths. Nat Photon, 2021, 15: 493–498
5 Wang Z, Wang X, Cong S, *et al.* Towards full-colour tunability of inorganic electrochromic devices using ultracompact Fabry-Perot nanocavities. Nat Commun, 2020, 11: 302
6 Davy NC, Sezen-Edmonds M, Gao J, *et al.* Pairing of near-ultraviolet solar cells with electrochromic windows for smart management of the

solar spectrum. Nat Energy, 2017, 2: 17104
7 Ponder JF, Österholm AM, Reynolds JR. Conjugated polyelectrolytes as water processable precursors to aqueous compatible redox active polymers for diverse applications: Electrochromism, charge storage, and biocompatible organic electronics. Chem Mater, 2017, 29: 4385–4392
8 Li D, Lai WY, Zhang YZ, *et al.* Printable transparent conductive films for flexible electronics. Adv Mater, 2018, 30: 1704738
9 Zhou L, Yu M, Chen X, *et al.* Screen-printed poly(3,4-ethylenedioxythiophene):poly(styrenesulfonate) grids as ITO-free anodes for flexible organic light-emitting diodes. Adv Funct Mater, 2018, 28: 1705955
10 Gu Z, Huang Z, Li C, *et al.* A general printing approach for scalable growth of perovskite single-crystal films. Sci Adv, 2018, 4: eaat2390
11 Gu Z, Zhou Z, Huang Z, *et al.* Controllable growth of high-quality inorganic perovskite microplate arrays for functional optoelectronics. Adv Mater, 2020, 32: 1908006
12 Gu Z, Huang Z, Hu X, *et al. In situ* inkjet printing of the perovskite single-crystal array-embedded polydimethylsiloxane film for wearable light-emitting devices. ACS Appl Mater Interfaces, 2020, 12: 22157–22162
13 Cheng T, Wu YW, Chen YL, *et al.* Inkjet-printed high-performance flexible micro-supercapacitors with porous nanofiber-like electrode structures. Small, 2019, 15: 1901830
14 Liu X, Yu Z, Yu M, *et al.* Iridium(III)-complexed polydendrimers for inkjet-printing oleds: The influence of solubilizing steric hindrance groups. ACS Appl Mater Interfaces, 2019, 11: 26174–26184
15 Derby B. Inkjet printing of functional and structural materials: Fluid property requirements, feature stability, and resolution. Annu Rev Mater Res, 2010, 40: 395–414
16 Kuang M, Wang L, Song Y. Controllable printing droplets for high-resolution patterns. Adv Mater, 2014, 26: 6950–6958
17 Yang G, Zhang YM, Cai Y, *et al.* Advances in nanomaterials for electrochromic devices. Chem Soc Rev, 2020, 49: 8687–8720
18 Li XG, Wang HY, Huang MR. Synthesis, film-forming, and electronic properties of *o*-phenylenediamine copolymers displaying an uncommon tricolor. Macromolecules, 2007, 40: 1489–1496
19 Pietsch M, Rödlmeier T, Schlisske S, *et al.* Inkjet-printed polymer-based electrochromic and electrofluorochromic dual-mode displays. J Mater Chem C, 2019, 7: 7121–7127
20 Chiolerio A, Bocchini S, Porro S. Inkjet printed negative supercapacitors: Synthesis of polyaniline-based inks, doping agent effect, and advanced electronic devices applications. Adv Funct Mater, 2014, 24: 3375–3383
21 Tang P, Xie L, Xiong X, *et al.* Realizing 22.3% EQE and 7-fold lifetime enhancement in QLEDs *via* blending polymer TFB and cross-linkable small molecules for a solvent-resistant hole transport layer. ACS Appl Mater Interfaces, 2020, 12: 13087–13095
22 Cai G, Darmawan P, Cheng X, *et al.* Inkjet printed large area multifunctional smart windows. Adv Energy Mater, 2017, 7: 1602598
23 Teo MY, Stuart L, Devaraj H, *et al.* The *in situ* synthesis of conductive polyaniline patterns using micro-reactive inkjet printing. J Mater Chem C, 2019, 7: 2219–2224
24 Hu G, Yang L, Yang Z, *et al.* A general ink formulation of 2D crystals for wafer-scale inkjet printing. Sci Adv, 2020, 6: eaba5029
25 Song D, Mahajan A, Secor EB, *et al.* High-resolution transfer printing of graphene lines for fully printed, flexible electronics. ACS Nano, 2017, 11: 7431–7439
26 Jang J, Ha J, Cho J. Fabrication of water-dispersible polyaniline-poly(4-styrenesulfonate) nanoparticles for inkjet-printed chemical-sensor applications. Adv Mater, 2007, 19: 1772–1775
27 Ngamna O, Morrin A, Killard AJ, *et al.* Inkjet printable polyaniline nanoformulations. Langmuir, 2007, 23: 8569–8574
28 Shim GH, Han MG, Sharp-Norton JC, *et al.* Inkjet-printed electrochromic devices utilizing polyaniline-silica and poly(3,4-ethylenedioxythiophene)-silica colloidal composite particles. J Mater Chem, 2008, 18: 594–601
29 Small WR, Masdarolomoor F, Wallace GG, *et al.* Inkjet deposition and characterization of transparent conducting electroactive polyaniline composite films with a high carbon nanotube loading fraction. J Mater Chem, 2007, 17: 4359–4361
30 Liu R, Fan S, Xiao D, *et al.* Free-standing single-molecule thick crystals consisting of linear long-chain polymers. Nano Lett, 2017, 17: 1655–1659
31 Li R, Ma X, Li J, *et al.* Flexible and high-performance electrochromic devices enabled by self-assembled 2D TiO_2/MXene heterostructures. Nat Commun, 2021, 12: 1587
32 Huang X, Niu Q, Fan S, *et al.* Highly oriented lamellar polyaniline with short-range disorder for enhanced electrochromic performance. Chem Eng J, 2021, 417: 128126
33 Barpuzary D, Kim K, Park MJ. Two-dimensional growth of large-area conjugated polymers on ice surfaces: High conductivity and photoelectrochemical applications. ACS Nano, 2019, 13: 3953–3963
34 Zhang T, Qi H, Liao Z, *et al.* Engineering crystalline quasi-two-dimensional polyaniline thin film with enhanced electrical and chemiresistive sensing performances. Nat Commun, 2019, 10: 4225
35 Choi IY, Lee J, Ahn H, *et al.* High-conductivity two-dimensional polyaniline nanosheets developed on ice surfaces. Angew Chem Int Ed, 2015, 54: 10497–10501
36 Bergin SD, Sun Z, Rickard D, *et al.* Multicomponent solubility parameters for single-walled carbon nanotube-solvent mixtures. ACS Nano, 2009, 3: 2340–2350
37 Cao Y, Smith P, Heeger AJ. Counter-ion induced processibility of conducting polyaniline and of conducting polyblends of polyaniline in bulk polymers. Synth Met, 1992, 48: 91–97
38 Li S, Cao Y, Xue Z. Soluble polyaniline. Synth Met, 1987, 20: 141–149
39 Shacklette LW, Han CC. Solubility and dispersion characteristics of polyaniline. MRS Proc, 1993, 328: 157–166
40 Andreatta A, Cao Y, Chiang JC, *et al.* Electrically-conductive fibers of polyaniline spun from solutions in concentrated sulfuric acid. Synth Met, 1988, 26: 383–389
41 Gul S, Shah AHA, Bilal S. Synthesis and characterization of processable polyaniline salts. J Phys-Conf Ser, 2013, 439: 012002
42 Huang K, Wan M. Self-assembled polyaniline nanostructures with photoisomerization function. Chem Mater, 2002, 14: 3486–3492
43 Wu CG, Yeh YR, Chen JY, *et al.* Electroless surface polymerization of ordered conducting polyaniline films on aniline-primed substrates. Polymer, 2001, 42: 2877–2885
44 Šeděnková I, Trchová M, Blinova NV, *et al. In-situ* polymerized polyaniline films. Preparation in solutions of hydrochloric, sulfuric, or phosphoric acid. Thin Solid Films, 2006, 515: 1640–1646
45 Basavaiah K, Pavankumar Y, Rao AVP. A facile one-step synthesis of PTSA-doped tetraaniline nanostructure/magnetite nanoparticles *via* self-assembly method. J Nanostruct Chem, 2013, 3: 74
46 Tkachenko LI, Nikolaeva GV, Ryabenko AG, *et al.* One-step synthesis of the polyaniline-single-walled carbon tubes nanocomposite in formic acid and its electrochemical properties. Prot Met Phys Chem Surf, 2018, 54: 617–623
47 Yue J, Epstein AJ. XPS study of self-doped conducting polyaniline and parent systems. Macromolecules, 1991, 24: 4441–4445
48 Shao Y, Fu JH, Cao Z, *et al.* 3D crumpled ultrathin 1T MoS_2 for inkjet printing of Mg-ion asymmetric micro-supercapacitors. ACS Nano, 2020, 14: 7308–7318
49 Weng SC, Fuh AYG, Tang FC, *et al.* Effect of surface condition on liquid crystal photoalignment by light-induced AZO dye adsorption phenomena. Liquid Crysts, 2016, 43: 1221–1229
50 Álvarez E, Vázquez G, Sánchez-Vilas M, *et al.* Surface tension of organic acids + water binary mixtures from 20°C to 50°C. J Chem Eng Data, 1997, 42: 957–960
51 Hu CW, Kawamoto T, Tanaka H, *et al.* Water processable Prussian blue-polyaniline:polystyrene sulfonate nanocomposite (PB-PANI:PSS) for multi-color electrochromic applications. J Mater Chem C, 2016, 4: 10293–10300
52 Cai G, Cheng X, Layani M, *et al.* Direct inkjet-patterning of energy efficient flexible electrochromics. Nano Energy, 2018, 49: 147–154
53 Zhang L, Chao D, Yang P, *et al.* Flexible pseudocapacitive electrochromics *via* inkjet printing of additive-free tungsten oxide nanocrystal ink. Adv Energy Mater, 2020, 10: 2000142
54 Yu F, Liu W, Ke SW, *et al.* Electrochromic two-dimensional covalent

organic framework with a reversible dark-to-transparent switch. Nat Commun, 2020, 11: 5534
55 Xia X, Chao D, Qi X, *et al.* Controllable growth of conducting polymers shell for constructing high-quality organic/inorganic core/shell nanostructures and their optical-electrochemical properties. Nano Lett, 2013, 13: 4562–4568
56 Choi C, Ashby DS, Butts DM, *et al.* Achieving high energy density and high power density with pseudocapacitive materials. Nat Rev Mater, 2020, 5: 5–19
57 Bai Z, Li R, Li K, *et al.* Transparent metal-organic framework-based gel electrolytes for generalized assembly of quasi-solid-state electrochromic devices. ACS Appl Mater Interfaces, 2020, 12: 42955–42961

Acknowledgements This work was supported by the International Cooperation Fund of the Science and Technology Commission of Shanghai (19520744500), the National Natural Science Foundation of China (51903045 and 52173031), the Program of Shanghai Academic/Technology Research Leader (20XD1400100), the Basic Research Project of the Science and Technology Commission of Shanghai (21JC1400100), and the Fundamental Research Funds for the Central Universities and Graduate Student Innovation Fund of Donghua University (CUSF-DH-D-2020048). We thank Dr. Renwei Liu (Shimadzu) for the help in AFM and XPS characterizations.

Author contributions Zhang Y and Fan S conceived and directed this research; Huang X performed the experiments, analyzed the data, and wrote the manuscript; Chen J conducted TEM and SAED measurements of PANI; Xie H performed the tensile and torsional experiments of ECDs; Zhao F constructed the screen-printed conductive silver line in the seven-segment display. The manuscript was written through the contributions of all authors. All authors gave approval to the final version of the manuscript.

Conflict of interest The authors declare that they have no conflict of interest.

Supplementary information Supporting data are available in the online version of the paper.

Xiangyu Huang is a PhD candidate at the College of Materials Science and Engineering, Donghua University (DHU). His current research interests are electrochromic devices and dynamic optical devices based on conjugated polymers.

Suna Fan is an associate professor at the College of Materials Science and Engineering, DHU. She received her PhD degree in materials physics and chemistry from Jilin University, in 2017. From 2017 to 2018, she was an assistant professor at Wenzhou Institute of Biomaterials and Engineering, Chinese Academy of Sciences (CAS) (renamed as Wenzhou Institute, University of CAS in 2019). She joined DHU in 2018. Her interest is focusing on conducting polymers and silk-based smart materials.

Yaopeng Zhang is a professor at the State Key Laboratory for Modification of Chemical Fibers and Polymer Materials, DHU. He received his PhD degree in materials science from DHU in 2002. From 2004 to 2007, he was a postdoctoral research fellow at Kawamura Institute of Chemical Research, Japan. He served as a visiting scholar at Akita University, Japan, and Stony Brook University, USA, respectively. His current research is focusing on silk materials for bioelectronic and biomedical applications.

用于柔性和图案化电致变色器件的二维聚苯胺的喷墨打印研究

黄翔宇, 陈杰, 谢鸿杰, 赵飞翔, 范苏娜*, 张耀鹏*

摘要 基于有机共轭聚合物的电致变色器件(ECD)在数字和彩色显示器中具有广阔的应用前景. 然而, 制备兼具优异电致变色性能、柔韧性和定制化图案的ECD仍然是一个挑战. 本文报道了利用喷墨打印技术制备二维层状聚苯胺(PANI)基柔性图案化ECD的方法. 层状PANI均匀分散在甲酸中, 能够实现高精度、稳定的喷墨打印. 同时, 层状PANI的纳米级厚度、适当的掺杂比例, 以及无添加剂的墨水成分, 使得打印后的PANI电极和器件保持较高的电致变色性能和电化学特性. 喷墨打印所得电极不仅表现出优异的光学对比度(76%, 750 nm波长)、良好的着色效率(259.1 $cm^2 C^{-1}$)、较短的着色/褪色时间(1.8/2.4 s), 而且具有赝电容特性与机械柔韧性. 此外, 本文所开发的二维层状PANI墨水可以定制化设计并打印成各种图案, 并以此制备电化学控制的可寻址电致变色显示器. 这种二维层状PANI电致变色材料可进一步用于柔性和图案化ECD, 在新型光电显示领域具有较好的应用前景.

